THE JOURNAL OF PHYSICAL CHEMISTRY B

Article

pubs.acs.org/JPCB

Manipulating Excited-State Dynamics of Individual Light-Harvesting Chromophores through Restricted Motions in a Hydrated Nanoscale Protein Cavity

Rodrigo Noriega,[†,‡] Daniel T. Finley,[†] John Haberstroh,[§] Phillip L. Geissler,[†,∥,⊥] Matthew B. Francis,[†,∥] and Naomi S. Ginsberg*[,†,∥,§,#,▽]

[†]Department of Chemistry, [‡]Energy Biosciences Institute, and [§]Department of Physics, University of California Berkeley, Berkeley, California 94720, United States

[∥]Materials Sciences Division, [⊥]Chemical Sciences Division, and [#]Physical Biosciences Division, Lawrence Berkeley National Laboratory, Berkeley, California 94720, United States

[▽]Kavli Energy NanoSciences Institute, Berkeley, California 94720, United States

Supporting Information

ABSTRACT: Manipulating the photophysical properties of light-absorbing units is a crucial element in the design of biomimetic light-harvesting systems. Using a highly tunable synthetic platform combined with transient absorption and time-resolved fluorescence measurements and molecular dynamics simulations, we interrogate isolated chromophores covalently linked to different positions in the interior of the hydrated nanoscale cavity of a supramolecular protein assembly. We find that, following photoexcitation, the time scales over which these chromophores are solvated, undergo conformational rearrangements, and return to the ground state are highly sensitive to their position within this cavity and are significantly slower than in a bulk aqueous solution. Molecular dynamics simulations reveal the hindered translations and rotations of water molecules within the protein cavity with spatial specificity. The results presented herein show that fully hydrated nanoscale protein cavities are a promising way to mimic the tight protein pockets found in natural light-harvesting complexes. We also show that the interplay between protein, solvent, and chromophores can be used to substantially tune the relaxation processes within artificial light-harvesting assemblies in order to significantly improve the yield of interchromophore energy transfer and extend the range of excitation transport. Our observations have implications for other important, similarly sized bioinspired materials, such as nanoreactors and biocompatible targeted delivery agents.

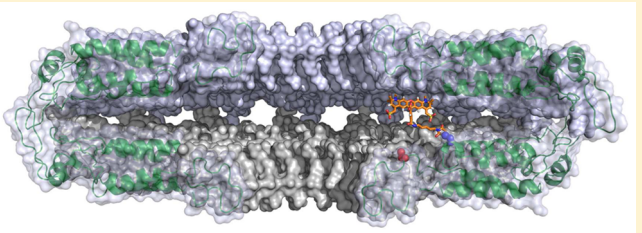

INTRODUCTION

In the first picoseconds of photosynthesis, photoexcitations originating in densely packed light-harvesting antennae—pigment-containing membrane proteins—travel with near unity quantum efficiency to the reaction center, where biochemistry is initiated.[1] Many of the design principles of this natural light harvesting remain to be elucidated. Yet, the remarkable efficiency with which photoexcitations propagate among pigments and between pigment-containing proteins results at least in part from the exquisitely evolved molecular environment provided to each chromophore by the surrounding protein.[1−10] This complex environment reduces both nonradiative and radiative losses of chromophore excitations so that they can travel efficiently between adjacent chromophores and so that these excitations can travel for a prolonged period before being quenched. One factor responsible for isolating photoexcitations and their chromophore hosts from a fluctuating and potentially lossy environment is that the pigments are often tightly enveloped by the protein.[8,9]

Because of the complexities associated with recreating such conformal protein "pockets"[11,12] the majority of attempts to mimic natural light harvesting involve linking pigment molecules to the exterior of a protein using flexible alkyl chains[13−16] or involve directly linking pigments to one another and dispensing with the protein entirely.[17−25] Here we present an alternate approach in which we create an effective pocket for chromophores by placing them within a nanoscale, hydrated cavity of a self-assembling protein scaffold. As a result of the fact that the water solvating the chromophores is also in close proximity to the protein surfaces that comprise the cavity, we control intra- and intermolecular fluctuations therein, as evidenced by transient absorption measurements and molecular dynamics simulations. Our observations reveal that all events in the photocycle of a chromophore can be substantially slowed relative to the chromophore's behavior in bulk water, even

Received: April 20, 2015
Revised: May 19, 2015

ACS Publications © XXXX American Chemical Society

DOI: 10.1021/acs.jpcb.5b03784
J. Phys. Chem. B XXXX, XXX, XXX−XXX

though there is a significant amount of water solvating both the protein cavity surface and the chromophore, in contrast to the typical hydrophobic protein pockets found in natural light harvesting.

The fluorophores used in biomimetic light harvesting can interact strongly with and perturb their environment. This situation is different from the desired role of smaller probes in the majority of studies of water dynamics near protein surfaces. The solvation dynamics of a small fluorescent probe 0.7 nm away from a protein surface have been measured to resemble behavior in bulk water.[26] Perturbations to other observables have been detected at larger distances up to ∼2 nm away from the protein/water interface. Extended hydration layers are supported by studies on the order parameter of the water network,[27] the orientational decorrelation of water molecules,[27,28] the rotation and translation dynamics of small paramagnetic probes,[29] the dipolar polarization of water,[30] or the collective motions of water in terahertz experiments.[30−33] In a related system, synthetic microenvironments such as host/guest or encapsulation complexes can also significantly affect the photophysics of fluorophores.[34,35] We show that the effects of a modified hydration layer inside a protein cavity can be used to tune the properties of biomimetic light harvesters.

The control that we demonstrate on isolated chromophores within a hydrated protein cavity represents a novel approach to tailoring their photophysical properties over a large dynamic range of time scales. The nanosecond fluorescence lifetime of flexible dyes in the cavity can be extended 3-fold, and the picosecond time scales for trapping on undesirable regions of the excited-state potential energy surface can be delayed by over an order of magnitude; both of these phenomena can facilitate highly desirable extended excitation transport. Even on the shorter time scales of photoinduced reorganization, the restricting, and hence slowing, effects of the protein surfaces and geometry can be felt by the chromophore and its innermost solvation shell on the order of 1 nm away from the protein surface. More generally, modifying the interplay between protein, solvent, and molecular solutes can dictate the thermodynamic state of a binding event in molecular recognition,[36,37] and it can play a large role in the activity of enzymes and chaperonins.[38−40] Therefore, the phenomena that we observe have general implications for the design of functional light-harvesting systems and can also have substantial effects in other types of similarly sized complexes, such as nanoreactors or targeted delivery agents.[41−47] The detailed measurements and modeling presented in this study reveal a new way in which synthetic control can be used to optimize protein−solvent−solute assemblies for functional gain.

APPROACH: SYNTHETIC CONTROL ENABLES THE PRECISE STUDY OF PROTEIN SUPRA-ASSEMBLIES

As a platform for our studies of spatially dependent chromophore−solvent−protein interactions we use the circular permutant of the tobacco mosaic virus (cpTMV) capsid protein (Figure 1).[48] The cpTMV protein self-assembles into two associated rings, each comprising 17 monomers. These assemblies have a C_2 symmetric double-ring structure with a cavity between the rings (Figure 1b, d) as revealed by X-ray crystallographic analysis.[48] A large amount of disorder in the central portion of the cpTMV double-rings precludes the complete determination of the structure of these protein assemblies. For the purpose of analysis, these disordered regions were modeled based on the positions of the equivalent

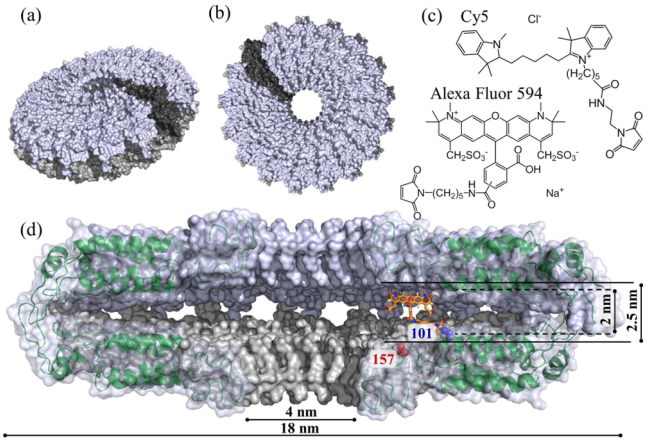

Figure 1. Circular permutant of the tobacco mosaic virus capsid protein. (a) The complete double-ring assembly, showing the molecular surface of the protein in pale blue for the upper half and in light gray for the lower half, with one protein monomer highlighted in dark gray. The modification sites are located along the surface of the interior cavity, shown in panel d. (b) Top view of the double-ring structure, clearly showing the pore that traverses the assembly. (c) Molecular structures of both fluorophores used in this study. (d) A cutaway down the middle of the assembly, showing the cavity between the protein rings. The ribbon representation of the monomers at the edge of the cut is shown in green. The positions of both available modification sites (157 in red, 101 in blue) are shown on one monomer, with the AF594 fluorophore in orange attached to the 101 residue. The dimensions of the assembly are also shown. As described in the text, the central regions of this structure (beyond the extent of the green helices) should be taken as highly disordered, and the positions of the backbone in these regions should only be used as guidelines.

residues in the wild-type double-ring TMV structure. Transmission electron microscopy of the cpTMV assemblies validates this assumption by showing the appropriate assembly dimensions and protein density in the pore.[48] This highly symmetric protein assembly ensures that all fluorophores placed on a given amino acid residue on any of the protein monomer units experience the same molecular environment. The entire structure measures 18 nm in diameter and 6 nm in height. The assembly has a doughnut shape (Figure 1b, d), with a 4 nm diameter "pore" traversing the rings at their center. The 8 nm deep cavity between the rings extends radially outward from the pore, and its height narrows gradually from 2.5 nm at the mouth of the cavity to 0.8 nm at the back of the cavity, furthest from the pore (Figure 1d). The circular permutant of the TMV capsid protein forms very stable double-rings (Supporting Information Figure S1), in comparison with the wider range of assembly states displayed by the wild-type protein.[48,49]

Controlled cysteine mutations to the protein's amino acid sequence allow the placement of maleimide-functionalized chromophores at specific locations in the cavity. Here, we access two different positions along the surface of the inner cavity of the cpTMV double-rings and designate each site by the location of the corresponding amino acid residue along the protein sequence (Figure 1d). Site 157 is located near the mouth of the cavity (adjacent to the pore), and site 101 is further recessed into the cavity (3 nm from the central opening). When used as a light-harvesting scaffold, the cpTMV double-rings are fully labeled with light-absorbing chromophores on every monomer.[48] In this study, however, we are

DOI: 10.1021/acs.jpcb.5b03784
J. Phys. Chem. B XXXX, XXX, XXX−XXX

interested in measuring the dynamics of individual fluorophores within the cavity with spatial specificity. We thus mutate only one residue at a time, and we avoid fluorophore−fluorophore interactions by using a very sparse labeling (≤0.01 dyes per protein monomer, Supporting Information Figure S2). These mutated cysteine residues are the only ones accessible for attachment on the entire cpTMV structure. This modification level is ideal for probing the molecular environment at different locations inside the narrowing protein cavity.

The combination of transient absorption and time-resolved fluorescence allows us to observe changes to the photophysical properties of fluorophores on time scales ranging from subpicosecond to tens of nanoseconds. To obtain a more complete picture of the molecular environment inside the cpTMV cavity, we study two different fluorophores with contrasting properties. We use a rhodamine derivative (Alexa Fluor 594, AF594) and an indocarbocyanine dye (Cy5). As a result of their distinct chemical structures (Figure 1c), these two dyes differ in the strength of their electric dipole moments, their conformational flexibilities, their fluorescence quantum yields, and their excited-state dynamics. Their linear absorption, emission, and excitation spectra are shown in Supporting Information Figure S3 along with the power spectra of the laser pulses used to measure their transient absorption. Rhodamines have a rigid xanthene core and, upon photoexcitation, have been shown to form a twisted intramolecular charge-transfer state by rotating the bond between their xanthene and phenyl moieties on a picosecond time scale.[50,51] Cyanine dyes are not inherently rigid molecules, and the intimate relation between structural rearrangements and the nonradiative deactivation of the excited state has been observed as a viscosity dependence of their nonradiative decay rates.[52] The solvation response of rhodamine dyes has a strong polar component, whereas cyanine dyes display a nonpolar solvation response.[53] The complementary and well-established photophysical properties of these fluorophores allow us to compare the different effects of hindered fluorophore−solvent motions inside a protein cavity on the molecular processes following photoexcitation. Studying the transient absorption, we access three different time scales on which the fluorophores' states evolve that report on different aspects of their molecular environments. These dynamics include the excited-state solvation, the subsequent intramolecular rearrangement, and the eventual fluorescence decay of the fluorophores.

In addition to these time-resolved measurements of the protein assemblies with complementary fluorophores, we similarly measure the fluorophore excited-state dynamics in bulk solvents of increasing viscosity, and we simulate the molecular dynamics of the hydrated protein assembly. Though the time-resolved measurements of the dyes in viscous bulk solvents cannot capture the heterogeneities of the protein cavity environment, they do mimic, albeit isotropically, the hindered rotation, translation, and rearrangement of solvent and solute molecules to provide a baseline to which we can compare and calibrate the magnitude of the cavity's effects on the excited-state dynamics that comprise the fluorophore photocycle. An increase in viscosity significantly hinders the motion of solvent and solute molecules by a combination of intermolecular interactions and excluded volume effects.[54] Glycerol has a polarity similar to water, but its viscosity is 3 orders of magnitude larger. By varying the volume fraction of glycerol in water, we tune the viscosity of the solvent mixture from 1 cP (0% glycerol) to a highly viscous value of 100 cP (85% glycerol). Indeed, it is necessary to employ this large dynamic range of bulk solvent viscosities in order to alter the fluorophore excited-state dynamics enough to mimic the slowing to time scales similar to those observed for fluorophores inside of the hydrated protein cavity.

We perform molecular dynamics simulations to characterize the molecular-scale processes taking place within the hydrated nanoscale protein cavity. These simulations include all 34 monomers of a complete double-ring protein assembly fully hydrated with explicit aqueous solvent, but do not include the fluorophores, as the development of suitable force fields is outside the scope of this study. We analyze the position and orientation of water molecules as a function of time for solvent molecule populations in different regions of the protein cavity. In combination, the time-resolved optical spectroscopy results and molecular dynamics simulations provide a remarkably detailed picture of the dynamic molecular environment in the protein assemblies.

Altogether, this study thus combines the measurement of the ultrafast excited-state dynamics of protein−fluorophore assemblies with the ability to experimentally control the location and identity of the fluorophores, the use of a tunable and highly symmetric protein scaffold, and the judicious comparison to isotropically hindered bulk viscous environments and to computer simulations. In this way, we provide an unprecedented window into the dynamics of solvent molecules and hydrated molecular solutes within protein assemblies at the nanoscale. These environment-dependent dynamics have large effects on the photophysical properties of fluorophores, with important implications for light harvester design.

METHODS

Sample Preparation and Characterization. Unless otherwise noted, all chemicals and solvents were of analytical grade and were used as received from commercial sources. Water used in biological procedures or as reaction solvent was deionized using a NANOpure purification system. Spin concentration steps were performed using 100 000 molecular weight cutoff spin concentrators from Millipore in an Eppendorf 5415 benchtop centrifuge. Large volume dialysis was performed with 3000 molecular weight cutoff SnakeSkin dialysis tubing. Small volume dialysis was performed with 3500 molecular weight cutoff Slide-A-Lyzer dialysis cassettes. Protein samples were quantified by the Bradford assay. Analytical size exclusion was performed on an Agilent 1100 series HPLC equipped with a PolySep-GFC-P 5000 column at a flow rate of 1 mL/min. Though retention times varied with the buffers used, protein rings typically eluted from 8 to 9 min, while protein monomers eluted from 9 to 10 min (Supporting Information Figure S1). Protein bioconjugates were analyzed using an Agilent 1200 series liquid chromatograph that was connected in-line with an Agilent 6224 time-of-flight (TOF) LC/MS system equipped with a Turbospray ion source. A gradient of water to acetonitrile, containing 0.1% formic acid over 20 min was used at a flow rate of 0.3 mL/min. Labeling yields were quantified by peak area integration (Supporting Information Figure S2). For samples where the fluorophores were not attached to the protein, they were capped with β-mercaptoethanol, a small thiol molecule (see Supporting Information text). Detailed procedures for protein expression, purification, and fluorophore bioconjugation can be found in the Supporting Information.

DOI: 10.1021/acs.jpcb.5b03784
J. Phys. Chem. B XXXX, XXX, XXX−XXX

Transient Absorption. An 80 MHz mode-locked Ti:sapphire Coherent Mantis oscillator was used to seed a 5 kHz Coherent Legend-Elite regenerative amplifier, whose output was split to pump either (1) a home-built noncollinear optical parametric amplifier or (2) an optical parametric amplifier (Coherent OPerA Solo) to produce laser light centered at 590 or 650 nm, respectively. Laser pulses with durations of 30−40 fs (after a folded prism compressor) were split into degenerate pump and probe pulses and focused to 100−150 μm diameter spot sizes (e^{-2} waist) inside a 1 mm path length quartz cuvette. The pump beam was routed through a variable-length path to control the pulse delay and chopped at 500 Hz for lock-in signal detection. Liquid samples with 1 mm path length optical densities at λ_{max} of 0.05 (AF594) and 0.1 (Cy5) were continuously circulated through the cuvette and a 1 mL reservoir with a peristaltic pump. Low energy fluences were used to prevent sample photodamage and nonlinearity in the observed dynamics (Supporting Information Figure S4). Effects of rotational reorientation of the excited molecules are avoided by setting pump and probe polarizations at the "magic angle" $\theta_m = 54.7°$. After passing through the sample, the transmitted beams were collimated, the pump beam was removed via spatial filtering, and the probe was focused onto an unbiased silicon photodiode. The output from the photodiode was split and coupled to two lock-in amplifiers: one to collect the raw transient absorption signal, ΔT, at the pump chopping frequency, and a second to collect the probe transmission signal, T, at the laser pulse repetition rate. The average signal and standard deviation (SD) for each sample were obtained from the collection of multiple scans while monitoring the signal amplitude for potential photobleaching. The flow rate of the sample recirculation pump was set so that the individual scans that we average together remained similar in strength from beginning to end of the experiment. Background scattering was subtracted, and the resulting traces were fit to a triexponential decay. Traces taken months apart are virtually indistinguishable (Supporting Information Figure S5).

Molecular Dynamics Simulations. The reported structure for the circular permutant of the TMV (PDB: 3KML) does not include those residues in strongly disordered sections of the structure. To obtain a complete structure as a starting point for our simulations, 3KML was merged with wild-type protein (PDB: 2TMV). The residues at positions 101 and 157 of the cpTMV were mutated to cysteines. Molecular dynamics simulations were run on GROMACS 4.6 with a hexagonal prism box of water with a hydration shell of 1.2 nm (2.4 nm between periodic replicas) surrounding the protein. A physiological concentration (0.255 mol/L) of NaCl was solvated into the water. During simulation, center-of-mass translation and rotation were removed from the protein. After a series of energy minimizations and equilibration runs, our analysis data was a 100 ps sample at 100 fs resolution at the end of a 10 ns equilibration trajectory. The analysis of static and dynamical order parameters in local regions was performed with the RMSDAnalyze python package written by the authors and described in the Supporting Information.

RESULTS: SLOWER EXCITED-STATE DYNAMICS WITHIN THE PROTEIN CAVITY AND IN VISCOUS SOLVENTS

In this section we first describe the measured excited-state dynamics of fluorophores placed at specific locations within the cpTMV protein cavity and in a range of bulk solvent mixtures of different viscosities. Their time-resolved population dynamics are observed by measuring the normalized change in transmission of a probe beam as a result of pump excitation, $\Delta T/T$, with transient absorption spectroscopy and the time-resolved fluorescence decays with time-correlated single-photon counting (see Supporting Information, Figures S6 and S7). These measurements show a pronounced effect of the hindered molecular motions on the excited-state population dynamics of the two dyes with complementary sensitivities discussed above. In this section, we also describe the results of molecular dynamics simulations of the supramolecular protein assembly with explicit aqueous solvent.

Time-Resolved Measurements. The transient absorption of AF594 and Cy5 in water, inside the protein cavity, and in water−glycerol mixtures are presented in Figure 2. The short

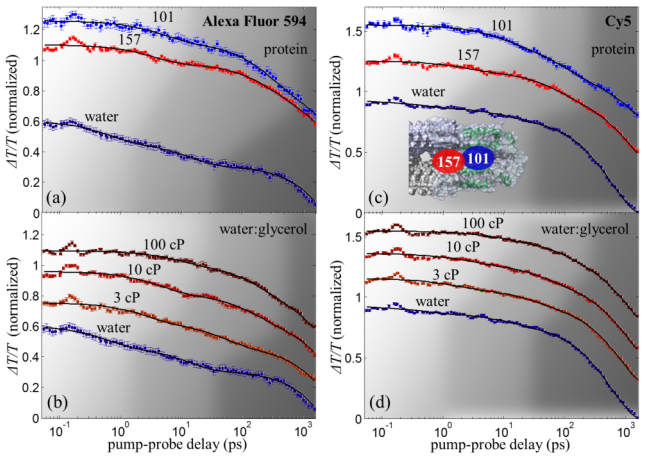

Figure 2. Transient absorption traces of a rigid and a flexible dye inserted in the cpTMV cavity and in bulk solvents. (a) Transient absorption traces for AF594 free in aqueous solution (purple) compared to inserted in the cavity of cpTMV protein rings at positions 157 (red) and 101 (blue). (b) Transient absorption traces for AF594 in solvents of increasing viscosity −1 cP (pure water) in purple, 3, 10, and 100 cP in light to dark brown. (c) Transient absorption traces for Cy5 free in aqueous solution (purple) compared to inserted in the cavity of cpTMV protein rings at positions 157 (red) and 101 (blue). (d) Transient absorption traces for Cy5 in solvents of increasing viscosity −1 cP (pure water) in purple, 3, 10, and 100 cP in light to dark brown. Inset: cross section of the protein cavity, displaying the fluorophore locations when labeling sites 157 (red) and 101 (blue). Error bars are ±1 SD of the mean from several measurements (see Methods). Typical values of $\Delta T/T$ are of the order of 10^{-3}. Normalized traces are displaced vertically for clarity. AF594 in water, −0.4; at site 157, +0.15; at site 101, +0.3; 3 cP, −0.2; 10 cP, 0; 100 cP, +0.15. Cy5 in water, −0.05; at site 157, +0.3; at site 101, +0.6; 3 cP, +0.2; 10 cP, +0.4; 100 cP, +0.6. Solid lines are triexponential fits. Shaded areas are guides to the eye, with a transition from light to dark gray demarcating the regions where each decay component is observed.

time oscillation in the transients due to the excitation of a vibrational wavepacket damps out quickly and was not included in our analysis. Each of the transient absorption traces for AF594 and Cy5 displays three distinct exponential decays, irrespective of environment. For AF594 in bulk water (Figure 2, parts a and b; purple traces), the transient absorption signal decays with a fast time constant of 0.6 ps, an intermediate time constant of 13 ps, and a long time constant of 3.9 ns. In bulk water, the transient absorption signal of Cy5 (Figure 2, parts c and d; purple traces) decays with a fast time constant of 0.4 ps,

DOI: 10.1021/acs.jpcb.5b03784
J. Phys. Chem. B XXXX, XXX, XXX−XXX

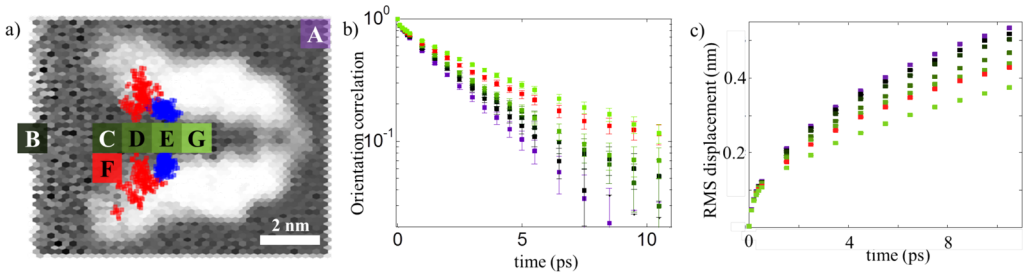

Figure 3. Molecular dynamics simulations of protein assemblies and explicit solvent. (a) Snapshot of the simulation box projected onto a two-dimensional representation parametrized by a molecule's distance radially outward from the center of the pore and the vertical distance from the plane of symmetry between the protein rings. The number of water molecules per unit volume is shown by the grayscale shading and is markedly different between the cavity (dark areas) and the protein scaffold (white areas). The positions of the atoms corresponding to sites 157 and 101 from each of the 34 protein monomers are shown as red and blue markers, respectively. Several regions of interest for the calculation of translation and rotation of water molecules within them are displayed as colored boxes (purple, black, dark to light green, and magenta) and labeled A–G. (b) Correlation function of the molecular orientation of solvent molecules originally within each of the boxed regions in panel a. The rotation of solvent molecules is slower deeper in the cavity and closer to the protein surface. (c) Root-mean-square displacement of the solvent molecules originating within each of the boxed regions in panel a. The displacement of solvent is slower deeper in the cavity and closer to the protein surface.

an intermediate time constant of 11 ps, and a long time constant of 572 ps.

When the fluorophores are inserted into the cpTMV protein cavity (Figure 2, parts a and c; red and blue traces) or are dissolved in viscous water–glycerol mixtures (Figure 2, parts b and d; brown traces), the time scales for all three decays are slower than in bulk water. The fast and intermediate decays are slowed down by over an order of magnitude for both fluorophores when comparing their values in bulk water to those in the most viscous solvents. The longer time-scale decay is slower by ~3× for Cy5, a flexible fluorophore, but it shows no change for AF594, a rigid fluorophore. The amplitudes and time constants obtained by fitting triexponential functions to the transient absorption for each sample are shown in Supporting Information Table S1. The differences we observe in the excited-state dynamics of the fluorophores when inserted into the protein cavity are due to variations in their molecular environment within the solvent–chromophore–protein assembly and not due to chemical modification in the protein labeling process or to noncovalent associations of the dye and protein (see Supporting Information text, Figures S8 and S9, and Tables S4–S6). It is known that hindered solvent motions result in retarded excited-state dynamics, and that a protein surface affects the motions of water molecules in its vicinity. Here we observe the effect that these phenomena have on individual chromophores at different positions within a nanoscale hydrated protein cavity and explore the changes in the various steps of their photocycle. Changes in the time scales for excited-state relaxation and decay have important implications when these fluorophores are used in a light-harvesting scaffold.

We defer to the following section a discussion of the molecular processes responsible for the observed dynamic signatures of the fluorophores and of how the trends displayed by the data relate to the effects of hindered fluorophore and solvent molecule motions within the protein cavity. Before this discussion, we first describe the molecular-scale properties of the environment within the protein cavity, which can be better understood through simulation.

Molecular Dynamics Simulations. Our molecular dynamics simulations allow us to observe, at the molecular scale, the dynamics of solvent molecules and of the protein scaffold. The grayscale in the image in Figure 3a represents the average number of solvent molecules per unit volume within cells of the simulation lattice as a function of axial and radial position. Darker areas represent regions occupied by water, and the region occupied by the protein is primarily white or very pale. The position of the atoms corresponding to residues at sites 157 and 101 in each of the 34 protein monomers of one protein assembly in a single simulation frame are shown in red and blue markers, respectively. As evidenced by the larger range of positions occupied by site 157 compared to the smaller distribution of positions displayed by site 101, the section of the protein where site 157 resides has a greater conformational flexibility. This result is in agreement with previous X-ray crystallography experiments.[48]

The molecular-scale detail provided by the molecular dynamics simulations allows us to analyze the motions of water molecules with spatial specificity within different regions of the assembly (A–G colored boxes in Figure 3a). For the collections of water molecules that are initially located within each of these boxed regions of the assembly, we calculate and plot the average autocorrelation of their orientations as a function of time (Figure 3b) as well as the average root-mean-squared (RMS) displacements (Figure 3c). Details can be found in the Supporting Information text. The distribution of values of RMS displacement and angular autocorrelation for the collection of molecules within each region of interest shows no signature of multiple subpopulations (Supporting Information Figure S10). It is thus valid to describe each distribution by its mean as a function of time. At short times, the motions of water molecules in each of the boxed regions in Figure 3a show the same behavior, but they subsequently diverge.

The water molecule orientational correlation curves in Figure 3b are fit to a biexponential function with a constant offset to account for time components longer than our simulation window (Supporting Information Table S7). The fast exponential decay has a time scale of ~140 fs and an amplitude of 12–16% for all sampled regions in our simulation. The considerable confidence intervals obtained for this fast component preclude the ability to determine a trend as a function of location in the cavity. The second time-scale component has the largest amplitude (75–86%) and shows significant variations among the boxed sampled regions within the simulation box. Its value is 2.18 ps for water molecules in the exterior of the cavity and away from the protein (A, purple in Figure 3), slowing down to 2.94 ps for solvent molecules close to the protein at the mouth of the cavity (F, magenta in

DOI: 10.1021/acs.jpcb.5b03784
J. Phys. Chem. B XXXX, XXX, XXX–XXX

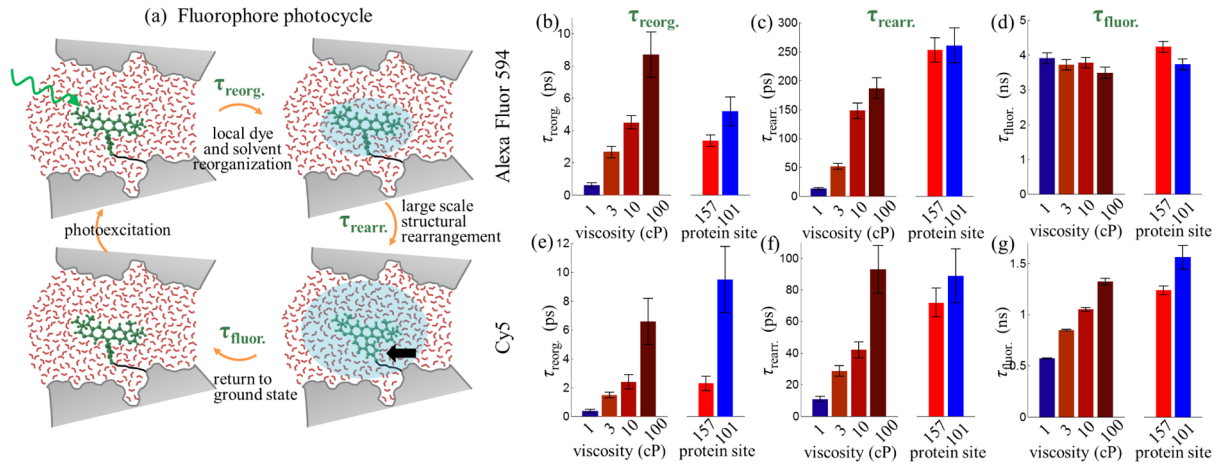

Figure 4. Fluorophore photocycle and associated time scales. (a) Sketch of the photocycle of a hydrated fluorophore inside a nanoscale protein cavity. The protein surface is shown in gray, water molecules in red, and the fluorophore in green. The flexible linker between the fluorophore and labeling site is in black. Relevant processes are labeled, with their associated time scales, between each "snapshot". The rough extents of solvent molecules involved are highlighted in blue. The bold arrow points to the region of the fluorophore undergoing structural rearrangement. Bar charts with the fitted time constants for each decay component of the transient absorption traces are shown in panels b–d for AF594 and e–g for Cy5. Error bars are ±1 SD of the fitted value.

Figure 3), and slowing even further to 3.80 ps for those water molecules deepest in the cavity (G, light green in Figure 3). Only for the regions that are close to a protein surface does the biexponential fit to the water molecule orientational correlation approach a nonzero value at long times (5–10% of initial value). The two distinct time scales of the angular decorrelation of water molecules in our simulation are in agreement with previous reports of faster librations combined with slower reorientational jumps and frame tumbling and are consistent with other studies of the dynamics of water molecules in the proximity of proteins.[55−60] Molecular dynamics studies of water–glycerol mixtures report a slowdown in the orientational rearrangements of water molecules by a factor of ∼10 for a ∼25% glycerol mixture,[61] which is larger than what we compute for water in proximity to the cpTMV protein surface.

The RMS displacements of the water molecules computed from the simulation data can be used to estimate water diffusion coefficients with spatial specificity within the protein assembly (see Supporting Information and Figure S11). We find unconstrained water molecules in the exterior of the cavity have a diffusion coefficient of 4.9×10^{-3} nm^2/ps (A, purple in Supporting Information Figure S11), in agreement with previous reports of bulk TIP3P water.[62] In mixtures of water and glycerol, molecular dynamics studies have found notable decreases in the translational diffusion of water molecules.[61] Here, we observe that water molecules near the protein at the mouth of the cavity have a smaller diffusion coefficient of 3.0×10^{-3} nm^2/ps (F, magenta in Supporting Information Figure S11), and water molecules deeper into the cavity have an even smaller diffusion coefficient of 2.3×10^{-3} nm^2/ps (G, light green in Supporting Information Figure S11).

DISCUSSION: EFFECTS OF HINDERED MOLECULAR MOTIONS ON THE FLUOROPHORE PHOTOCYCLE

To best interpret how the transient absorption time scales are extended when the fluorophores are inserted into the hydrated protein cavity, we associate each of the components of the triexponential behavior with a molecular-scale process, in agreement with previous ultrafast studies on rhodamines[50,51] (AF594) and on cyanines[52,53] (Cy5). The photoexcitation of the fluorophore can be considered to be instantaneous for the ∼35 fs time resolution of our apparatus and results in a change in the fluorophore's electronic configuration from the ground state to the excited state. The three exponential components of the transient absorption signal are interpreted as follows: (i) the fast component (τ_{reorg} ∼ 0.1–10 ps) is due to the reorganization of the photoexcited fluorophore and the solvent molecules in its immediate vicinity, (ii) the intermediate component (τ_{rearr} ∼ 10–100 ps) is related to larger-scale rearrangements of the chromophore and the coordinated displacement of solvent molecules, and (iii) the long component (τ_{fluor} ∼ 100 ps to 1 ns) reflects the fluorophore's return to the ground state. This cycle of creation, stabilization, and decay of the excited state of a fluorophore is sketched in Figure 4a. The values for the time constants obtained by fitting triexponential functions to the transient absorption traces (Supporting Information Table S1) are graphically displayed in Figure 4b–g, are grouped by the process in the photocycle that they represent, and are sequentially discussed below. Each of the dynamic time scales that we observe illustrates a different aspect of the interactions between protein, solvent, and fluorophores in the hindered environment of a nanoscale cavity. We compare these dynamic time scales to those that we observe for rotational decorrelation and translations in molecular dynamics simulations. Although we cannot do so in absolute terms due to the absence of the chromophore in the simulations, the trends in the corresponding experimental and simulated values agree with one another.

Reorganization after Fluorophore Photoexcitation. As is well-known, after an "instantaneous" change in a fluorophore's electric dipole moment, its solvation shell reacts with a subpicosecond rearrangement of the dipole moments of solvent molecules. The nuclear coordinates of the fluorophore also undergo a short-range reorganization as they evolve away from the Franck–Condon region of the excited-state potential energy surface. Our experiments do not directly measure the solvation correlation function as in photon echo or fluorescence upconversion experiments.[63−71] We do, however, observe the stabilization of the excited state and the concomitant change in

DOI: 10.1021/acs.jpcb.5b03784
J. Phys. Chem. B XXXX, XXX, XXX–XXX

the transient absorption signal. In bulk water and water-glycerol mixtures, the isotropic hindrance of solvent and fluorophore molecules induced by increasing the solvent viscosity up to 100 cP causes a slowdown of this ultrafast reorganization by up to 16× (Figure 4, parts b and e; purple- and brown-shaded bars). When the hydrated fluorophores are positioned inside the protein cavity, they display significantly slower reorganization dynamics than in bulk water. More significantly, these dynamics are strongly determined by the position of the fluorophore within the cavity. At the mouth of the cavity, both fluorophores display a 5× slower reorganization (red bars). The reorganization time scale increases by 9× for AF594 in the innermost probed position of the cavity (blue bar) over that in bulk water. At this same position, the time scale increases by 25× for Cy5. This difference in the degree of retardation of the local reorganization of the fluorophores and solvent deep in the protein cavity is likely due to how the fluorophores' polarities affect their solvation responses. AF594 is primarily polar (a similar dye, Texas Red, has a permanent dipole moment of 21 D[72]), while Cy5 is primarily nonpolar (symmetric indocarbocyanine dyes have been found to have negligible permanent dipole moments[73]). However, the overall trend for both fluorophores is that the reorganization upon photoexcitation slows progressively as the fluorophore is inserted deeper into the narrowing cavity.

The local reorganization of the hydration shell surrounding the fluorophore requires the rotation of water molecules, similar to the reorientation of water molecules in our simulations. The response of nonpolar solutes has been shown to be coupled to the translational motion of solvent molecules, which we also observe in our molecular dynamics simulations. In our molecular dynamics simulations, the rotations and translations of water molecules deep in the cavity or near the protein surface are significantly hindered as evidenced by their slower angular decorrelation (Figure 3b) and smaller RMS displacements (Figure 3c). The increases in the experimentally measured time constants for reorganization (in Figure 4, parts b and e) are ∼4× times larger than the increases observed in the molecular dynamics simulations. The absence of the fluorophore in our simulations most likely accounts for the discrepancy with experiment, since including the fluorophore would displace a significant volume of solvent and impose additional constraints on the motions of water molecules, likely resulting in even slower dynamics.

This reorganization involves predominantly the fluorophore and those water molecules in the nearest hydration shell. While the ∼1 nm flexible linker connecting the fluorophore and the protein may not be fully extended, the similarity in the transient absorption traces for the dye−protein mixtures without covalent attachment and those for the dye in bulk water indicate a low nonspecific affinity between dyes and the protein surface. Though it is conceivable that the covalently linked dyes are able to interact directly with the protein residues on the cavity walls, we conclude that the fluorophores are primarily solvated by water in the cavity. This solvation shell is, however, affected by their proximity to the cavity walls. It has been proposed that a protein affects the dynamics of the hydration layer around it through interactions between the charged residues at the protein surface and the water molecule dipoles.[28,30] The majority of the residues on the surface of the cpTMV cavity are neutral, but there is a larger number of both positively and negatively charged residues at the back of the cavity (Supporting Information Figure S12) that are not surprisingly involved in the electrostatic interactions required for supramolecular assembly. This charge distribution could corroborate the stronger retardation observed deep inside the cavity. These results suggest that a nanoscale hydrated protein cavity is a promising platform to design environments that mimic natural protein pockets.

Rearrangement of Fluorophore and Solvent Molecules. After the initial reorganization of the photoexcited fluorophores and the solvent molecules that surround them, the fluorophores both undergo a slower relaxation process on the excited-state energy surface that includes structural rearrangements and more substantial solvent displacement. In bulk solutions with free dye molecules, we observe that increasing the viscosity of the solvent results in a gradual slowdown of these molecular rearrangements for both the flexible and rigid fluorophores from ∼10 ps in water to ∼100 ps in the most viscous 100 cP solvent (Figure 4, parts c and f; purple and brown bars). When the fluorophores are positioned inside the protein cavity (red and blue bars), they experience significantly slower relaxation dynamics than in bulk water, but there is little difference between the two positions within the cavity. In the case of AF594, we measure 253 ± 21 ps at the mouth of the cavity and 261 ± 30 ps deeper in the cavity; for Cy5 we measure 72 ± 9 ps and 89 ± 17 ps, respectively. This process is slowed roughly 3 times more for the AF594 molecule than for Cy5. This difference could be due to the AF594 molecule's change in charge distribution to form a twisted intramolecular charge-transfer state,[50,51] but is most likely due to the corresponding twist of the bond between the rigid xanthene and phenyl moieties, in contrast to the rearrangements of multiple flexible bonds present in Cy5.

These larger molecular rearrangements necessitate the displacement of water molecules beyond the nearest hydration shell. Such displacements are subject to the time scales on which the solvent can flow over comparable distances; therefore, it is useful to compare the experimental observations to the spatially dependent diffusion coefficients calculated with molecular dynamics simulations (Supporting Information Figure S11). While the general trend in the calculated diffusion coefficients is to slow solvent flow in the cavity, the effects are again smaller in the simulations than in the time-resolved measurements.

In general, the reversibility of this sort of relaxation process is likely to be limited, and the change in dipole moment may be quite significant, especially if the final state has a charge-transfer character like for AF594. Our measurements show that these large-scale rearrangements can be slowed to time scales comparable to those in which energy is transferred between adjacent pigments in artificial light harvesters.[74] The observation of a significantly slower excited-state rearrangement of a pigment within a hydrated nanoscale protein cavity can have significant implications for the use of these structures as light-harvesting scaffolds: If the interchromophore coupling decreases as a result of this rearrangement process, placing the chromophores in nanoscale protein cavities presents a strategy to enable energy transfer to adjacent molecules to more favorably compete with trapping in these less desirable excited states.

Return of the Photoexcited Fluorophore to Its Ground State. Generally, a combination of radiative and nonradiative pathways determines the rate of return of a photoexcited fluorophore to its ground state. The fluorescence lifetime of flexible dyes is typically shorter than that of rigid

DOI: 10.1021/acs.jpcb.5b03784
J. Phys. Chem. B XXXX, XXX, XXX−XXX

molecules, as their conformational flexibility results in larger nonradiative decay rates. This connection between conformational flexibility and nonradiative decay is evident in the different trends we observe for the fluorescent lifetime of the fluorophores as their molecular environment is modified. On the one hand, the fluorescence lifetime of AF594 is essentially invariant to its environment (Figure 4d) since the intramolecular motions of its rigid structure that could contribute to internal conversion are already minimal, irrespective of its environment. On the other hand, Cy5 is more flexible and displays considerable variations in its fluorescence lifetime depending on its environment. For isolated Cy5 in bulk solvents, the fluorescence lifetime increases from 572 ps in water to 1.33 ns in the most viscous, 100 cP, solvent (Figure 4g, purple and brown bars). The fluorescence lifetime of Cy5 is also sensitive to its location within the protein cavity, increasing to 1.24 ns at the mouth of the cavity (red) and further increasing to 1.56 ns deeper inside the cavity (blue).

We interpret the increase in the fluorescence lifetime of Cy5 inside the hydrated protein cavity as resulting from a hindrance of molecular motions of the excited fluorophore and the surrounding solvent. These hindered molecular motions are likely to result from the typical slower motions of aqueous solutions near the surface of proteins and from the resulting constraints that these hindered water molecules impose on the fluorophores. They prevent the crossover to regions of the excited-state surface where internal conversion is more efficient, and thus extend the fluorescence lifetime. This interpretation is consistent with the previously observed decrease in the nonradiative rate of cyanines[52] and other flexible dyes[54] in viscous solvents. It is also possible, however, that the radiative decay rate of the fluorophore is affected by its proximity to polarizable protein residues.

The ability of a photoexcitation to migrate long distances in a chromophore array is dependent on the competition between two rates: the rate at which it is transferred between adjacent units and the rate at which it decays back to the ground state. The ability to increase the lifetime of excitations by tuning the molecular environment of the chromophores within the assembly can thus significantly increase the distance over which these excitations can diffuse and be efficiently collected. For example, if an excitation would migrate via an unbiased random walk on a circular arrangement of chromophores fully labeling either the 101 or 157 sites of a cpTMV supra-assembly, the 2.7× enhancement of the photoexcitation lifetime that we have observed here would result in an increase in collection efficiency of 65%.

CONCLUSIONS: LIGHT-HARVESTING DESIGN SHOULD TAKE ADVANTAGE OF A CHROMOPHORE'S INTERACTIONS WITH ITS SURROUNDINGS

By controlling the attachment point of individual fluorophores in the hydrated cavity of a self-assembled supramolecular protein assembly, we have demonstrated that this nanoscale molecular environment has substantial effects on the fluorophore photocycle. Through transient absorption and fluorescence measurements, we found that all processes that comprise the photocycle can be significantly slowed for the fluorophores in the cavity by up to 25× those measured in bulk water. Furthermore, we found that the measured time scales can even exceed those measured for isolated fluorophores in bulk solutions 100× more viscous than bulk water. Moreover, the variations in dynamics are highly sensitive to the fluorophore identity and to the placement of the fluorophore in the cavity, with the most dramatic slowing measured occurring in regions where the opposing cavity walls are closest to one another though still ∼2 nm apart. We also found through molecular dynamics simulations of the hydrated protein assembly that the slowing of the fluorophore's excited-state dynamics is related to hindered rotations and translations of water molecules near the cavity's protein surface. Analyzing the cavity effects on each step in the fluorophore photocycle has allowed us to suggest strategies for improving the properties of artificial light-harvesting systems, as described below.

First, the usual strategy when selecting bright pigments for artificial light harvesting is to use rigid molecules that must often be specially synthesized or carefully handled due to poor photostability. As shown here, rigidification that enhances fluorescence lifetimes can be built into the environment instead of into the molecule itself. This rigidification could thus enhance the viability of more common dye molecules with strong absorption or facile coupling to one another when they might otherwise be discarded on the basis of low fluorescent yields and short lifetimes. Furthermore, engineering a cavity within a de novo protein complex to manipulate dye photophysics is a challenging feat, but taking advantage of the naturally occurring self-assembly of individual monomers used in this study enables the facile formation of such a cavity.

Next, in natural light harvesters, energy migration happens on time scales much faster than the relaxation of the excited state due to the strong coupling between chromophores. Artificial systems thus far generally operate in a weaker coupling regime, where energy migration happens through incoherent hops. In this work we have presented evidence that, within a nanoscale protein cavity, large-scale molecular rearrangements of the excited fluorophore that require displacement of a significant amount of solvent are slowed to time scales that are comparable to those for energy transfer between adjacent fluorophores via incoherent hopping.[74] Delaying an individual fluorophore's evolution to such traps on the excited-state landscape can ensure that excitation transfer to adjacent fluorophores in the light-harvesting complex occurs prior to trapping. Furthermore, extending the time scale for relaxation to the ground state enables many more of such individual transfer events to occur, thus extending the range of excitation migration. A tunable system, such as the one described here, where the interchromophore couplings can be engineered by the position of adjacent fluorophores, and where the relaxation within and from the excited-state manifold is significantly slowed by the fluorophore's molecular environment, presents a unique opportunity to design artificial light-harvesting systems that emulate the "transfer before relaxing" behavior that is a hallmark of natural light-harvesting structures.

Last, we have observed dramatic changes to the ultrafast reorganization dynamics of the fluorophore and its immediate hydration layer within the protein cavity, showing that the protein surface can have significant effects even at large distances. Thus, a nanoscale hydrated protein cavity is a promising platform to design molecular environments that mimic the effects of natural protein pockets. These characteristics of the molecular environment inside nanoscale protein cavities are general and have implications for protein-based reaction vessels and targeted delivery agents, where constricted

DOI: 10.1021/acs.jpcb.5b03784
J. Phys. Chem. B XXXX, XXX, XXX−XXX

environments with slow solvent rearrangements may prove useful for stabilizing intermediate species or noncovalent complexes.

In sum, we have shown that, in artificial light-harvesting systems based on supramolecular protein assemblies, engineering the appropriate molecular environment represents a novel and previously unexplored way to substantially tailor the excited-state properties of the light absorbing units as well as their couplings. The flexibility afforded by the synthetic control of labeling sites and densities in our artificial light-harvesting assembly enables the characterization of chromophore−environment interactions at different labeling locations by eliminating the coupling between chromophores. Thus, deconstructing biomimetic light harvesters could provide valuable insights into the elusive light-harvesting design principles that have evolved in nature, where the effects of the chromophore environment are difficult to deconvolve from chromophore−chromophore coupling in spectroscopic measurements. In future designs of biomimetic light-harvesting systems, we anticipate that the integration of the variations in the molecular environment within protein cavities will provide a previously unexploited additional control in order to achieve optimal performance.

■ ASSOCIATED CONTENT

Supporting Information

Detailed synthesis and characterization of samples, as well as supporting experiments and computational methods. The Supporting Information is available free of charge on the ACS Publications website at DOI: 10.1021/acs.jpcb.5b03784.

■ AUTHOR INFORMATION

Corresponding Author

*E-mail: nsginsberg@berkeley.edu.

Notes

The authors declare no competing financial interest.

■ ACKNOWLEDGMENTS

This work was supported by the Director, Office of Science, Chemical Sciences, Geosciences, and Biosciences Division, of the U.S. Department of Energy under Contract No. DEAC02-05CH1123. Time-resolved fluorescence at the Lawrence Berkeley Laboratory Molecular Foundry was performed as part of the Molecular Foundry user program, supported by the Office of Science, Office of Basic Energy Sciences, of the U.S. Department of Energy under Contract No. DE-AC02-05CH11231. R.N. gratefully acknowledges financial support through a Philomathia Foundation Postdoctoral Fellowship, and N.S.G. acknowledges a David and Lucile Packard Foundation Fellowship for Science and Engineering.

■ REFERENCES

(1) Blankenship, R. E. *Molecular Mechanisms of Photosynthesis*; Blackwell Science: Oxford, U.K., 2002.

(2) Collini, E.; Wong, C. Y.; Wilk, K. E.; Curmi, P. M. G.; Brumer, P.; Scholes, G. D. Coherently Wired Light-Harvesting in Photosynthetic Marine Algae at Ambient Temperature. *Nature* **2010**, *463*, 644−647.

(3) Panitchayangkoon, G.; Hayes, D.; Fransted, K. A.; Caram, J. R.; Harel, E.; Wen, J.; Blankenship, R. E.; Engel, G. S. Long-Lived Quantum Coherence in Photosynthetic Complexes at Physiological Temperature. *Proc. Natl. Acad. Sci. U. S. A.* **2010**, *107*, 12766−12770.

(4) Tiwari, V.; Peters, W. K.; Jonas, D. M. Electronic Resonance with Anticorrelated Pigment Vibrations Drives Photosynthetic Energy Transfer Outside the Adiabatic Framework. *Proc. Natl. Acad. Sci. U. S. A.* **2013**, *110*, 1203−1208.

(5) Fuller, F. D.; Pan, J.; Gelzinis, A.; Butkus, V.; Senlik, S. S.; Wilcox, D. E.; Yocum, C. F.; Valkunas, L.; Abramavicius, D.; Ogilvie, J. P. Vibronic Coherence in Oxygenic Photosynthesis. *Nat. Chem.* **2014**, *6*, 706−711.

(6) Christensson, N.; Kauffmann, H. F.; Pullerits, T.; Mančal, T. Origin of Long-Lived Coherences in Light-Harvesting Complexes. *J. Phys. Chem. B* **2012**, *116*, 7449−7454.

(7) Scholes, G. D.; Fleming, G. R.; Olaya-Castro, A.; van Grondelle, R. Lessons from Nature About Solar Light Harvesting. *Nat. Chem.* **2011**, *3*, 763−774.

(8) Lee, H.; Cheng, Y.-C.; Fleming, G. R. Coherence Dynamics in Photosynthesis: Protein Protection of Excitonic Coherence. *Science* **2007**, *316*, 1462−1465.

(9) Curutchet, C.; Kongsted, J.; Muñoz-Losa, A.; Hossein-Nejad, H.; Scholes, G. D.; Mennucci, B. Photosynthetic Light-Harvesting Is Tuned by the Heterogeneous Polarizable Environment of the Protein. *J. Am. Chem. Soc.* **2011**, *133*, 3078−3084.

(10) Renger, T. Theory of Excitation Energy Transfer: From Structure to Function. *Photosynth. Res.* **2009**, *102*, 471−485.

(11) Farid, T. A.; Kodali, G.; Solomon, L. A.; Lichtenstein, B. R.; Sheehan, M. M.; Fry, B. A.; Bialas, C.; Ennist, N. M.; Siedlecki, J. A.; Zhao, Z.; et al. Elementary Tetrahelical Protein Design for Diverse Oxidoreductase Functions. *Nat. Chem. Biol.* **2013**, *9*, 826−833.

(12) Cohen-Ofri, I.; van Gastel, M.; Grzyb, J.; Brandis, A.; Pinkas, I.; Lubitz, W.; Noy, D. Zinc-Bacteriochlorophyllide Dimers in De Novo Designed Four-Helix Bundle Proteins. A Model System for Natural Light Energy Harvesting and Dissipation. *J. Am. Chem. Soc.* **2011**, *133*, 9526−9535.

(13) Miller, R. A.; Presley, A. D.; Francis, M. B. Self-Assembling Light-Harvesting Systems from Synthetically Modified Tobacco Mosaic Virus Coat Proteins. *J. Am. Chem. Soc.* **2007**, *129*, 3104−3109.

(14) Springer, J. W.; Parkes-Loach, P. S.; Reddy, K. R.; Krayer, M.; Jiao, J.; Lee, G. M.; Niedzwiedzki, D. M.; Harris, M. A.; Kirmaier, C.; Bocian, D. F.; et al. Biohybrid Photosynthetic Antenna Complexes for Enhanced Light-Harvesting. *J. Am. Chem. Soc.* **2012**, *134*, 4589−4599.

(15) Nam, Y. S.; Shin, T.; Park, H.; Magyar, A. P.; Choi, K.; Fantner, G.; Nelson, K. A.; Belcher, A. M. Virus-Templated Assembly of Porphyrins into Light-Harvesting Nanoantennae. *J. Am. Chem. Soc.* **2010**, *132*, 1462−1463.

(16) Endo, M.; Fujitsuka, M.; Majima, T. Porphyrin Light-Harvesting Arrays Constructed in the Recombinant Tobacco Mosaic Virus Scaffold. *Chem.—Eur. J.* **2007**, *13*, 8660−8666.

(17) Parkinson, P.; Knappke, C. E. I.; Kamonsutthipaijit, N.; Sirithip, K.; Matichak, J. D.; Anderson, H. L.; Herz, L. M. Ultrafast Energy Transfer in Biomimetic Multistrand Nanorings. *J. Am. Chem. Soc.* **2014**, *136*, 8217−8220.

(18) Ziessel, R.; Ulrich, G.; Haefele, A.; Harriman, A. An Artificial Light-Harvesting Array Constructed from Multiple Bodipy Dyes. *J. Am. Chem. Soc.* **2013**, *135*, 11330−11344.

(19) Wasielewski, M. R. Self-Assembly Strategies for Integrating Light Harvesting and Charge Separation in Artificial Photosynthetic Systems. *Acc. Chem. Res.* **2009**, *42*, 1910−1921.

(20) Gilat, S. L.; Adronov, A.; Fréchet, J. M. J. Light Harvesting and Energy Transfer in Novel Convergently Constructed Dendrimers. *Angew. Chem., Int. Ed.* **1999**, *38*, 1422−1427.

(21) Devadoss, C.; Bharathi, P.; Moore, J. S. Energy Transfer in Dendritic Macromolecules: Molecular Size Effects and the Role of an Energy Gradient. *J. Am. Chem. Soc.* **1996**, *118*, 9635−9644.

(22) Balzani, V.; Ceroni, P.; Maestri, M.; Vicinelli, V. Light-Harvesting Dendrimers. *Curr. Opin. Chem. Biol.* **2003**, *7*, 657−665.

(23) Weil, T.; Reuther, E.; Müllen, K. Shape-Persistent, Fluorescent Polyphenylene Dyads and a Triad for Efficient Vectorial Transduction of Excitation Energy. *Angew. Chem., Int. Ed.* **2002**, *41*, 1900−1904.

(24) Choi, M.-S.; Yamazaki, T.; Yamazaki, I.; Aida, T. Bioinspired Molecular Design of Light-Harvesting Multiporphyrin Arrays. *Angew. Chem., Int. Ed.* **2004**, *43*, 150−158.

DOI: 10.1021/acs.jpcb.5b03784
J. Phys. Chem. B XXXX, XXX, XXX−XXX

(25) Kodis, G.; Terazono, Y.; Liddell, P. A.; Andréasson, J.; Garg, V.; Hambourger, M.; Moore, T. A.; Moore, A. L.; Gust, D. Energy and Photoinduced Electron Transfer in a Wheel-Shaped Artificial Photosynthetic Antenna-Reaction Center Complex. *J. Am. Chem. Soc.* **2006**, *128*, 1818−1827.
(26) Pal, S. K.; Peon, J.; Zewail, A. H. Biological Water at the Protein Surface: Dynamical Solvation Probed Directly with Femtosecond Resolution. *Proc. Natl. Acad. Sci. U. S. A.* **2002**, *99*, 1763−1768.
(27) Ghosh, R.; Banerjee, S.; Hazra, M.; Roy, S.; Bagchi, B. Sensitivity of Polarization Fluctuations to the Nature of Protein-Water Interactions: Study of Biological Water in Four Different Protein-Water Systems. *J. Chem. Phys.* **2014**, *141*, 22D531.
(28) Martin, D. R.; Matyushov, D. V. Hydration Shells of Proteins Probed by Depolarized Light Scattering and Dielectric Spectroscopy: Orientational Structure Is Significant, Positional Structure Is Not. *J. Chem. Phys.* **2014**, *141*, 22D501.
(29) Franck, J. M.; Scott, J. A.; Han, S. Nonlinear Scaling of Surface Water Diffusion with Bulk Water Viscosity of Crowded Solutions. *J. Am. Chem. Soc.* **2013**, *135*, 4175−4178.
(30) Heyden, M.; Tobias, D. J.; Matyushov, D. V. Terahertz Absorption of Dilute Aqueous Solutions. *J. Chem. Phys.* **2012**, *137*, 235103.
(31) Heyden, M.; Tobias, D. J. Spatial Dependence of Protein-Water Collective Hydrogen-Bond Dynamics. *Phys. Rev. Lett.* **2013**, *111*, 218101.
(32) Ebbinghaus, S.; Kim, S. J.; Heyden, M.; Yu, X.; Heugen, U.; Gruebele, M.; Leitner, D. M.; Havenith, M. An Extended Dynamical Hydration Shell Around Proteins. *Proc. Natl. Acad. Sci. U. S. A.* **2007**, *104*, 20749−20752.
(33) Sushko, O.; Dubrovka, R.; Donnan, R. S. Sub-Terahertz Spectroscopy Reveals that Proteins Influence the Properties of Water at Greater Distances than Previously Detected. *J. Chem. Phys.* **2015**, *142*, 055101.
(34) Dsouza, R. N.; Pischel, U.; Nau, W. M. Fluorescent Dyes and Their Supramolecular Host/Guest Complexes with Macrocycles in Aqueous Solution. *Chem. Rev.* **2011**, *111*, 7941−7980.
(35) Ajami, D.; Rebek, J., Jr. More Chemistry in Small Spaces. *Acc. Chem. Res.* **2012**, *46*, 990−999.
(36) Baron, R.; Setny, P.; McCammon, J. A. Water in Cavity-Ligand Recognition. *J. Am. Chem. Soc.* **2010**, *132*, 12091−12097.
(37) Chodera, J. D.; Mobley, D. L. Entropy-Enthalpy Compensation: Role and Ramifications in Biomolecular Ligand Recognition and Design. *Annu. Rev. Biophys.* **2013**, *42*, 121−142.
(38) Grossman, M.; Born, B.; Heyden, M.; Tworowski, D.; Fields, G. B.; Sagi, I.; Havenith, M. Correlated Structural Kinetics and Retarded Solvent Dynamics at the Metalloprotease Active Site. *Nat. Struct. Mol. Biol.* **2011**, *18*, 1102−1108.
(39) Yang, L.; Dordick, J. S.; Garde, S. Hydration of Enzyme in Nonaqueous Media Is Consistent with Solvent Dependence of Its Activity. *Biophys. J.* **2004**, *87*, 812−821.
(40) England, J. L.; Pande, V. S. Potential for Modulation of the Hydrophobic Effect Inside Chaperonins. *Biophys. J.* **2008**, *95*, 3391−3399.
(41) Klem, M. T.; Willits, D.; Solis, D. J.; Belcher, A. M.; Young, M.; Douglas, T. Bio-inspired Synthesis of Protein-Encapsulated CoPt Nanoparticles. *Adv. Funct. Mater.* **2005**, *15*, 1489−1494.
(42) Bode, S. A.; Minten, I. J.; Nolte, R. J. M.; Cornelissen, J. J. L. M. Reactions Inside Nanoscale Protein Cages. *Nanoscale* **2011**, *3*, 2376−2389.
(43) Renggli, K.; Baumann, P.; Langowska, K.; Onaca, O.; Bruns, N.; Meier, W. Selective and Responsive Nanoreactors. *Adv. Funct. Mater.* **2011**, *21*, 1241−1259.
(44) Meldrum, F. C.; Wade, V. J.; Nimmo, D. L.; Heywood, B. R.; Mann, S. Synthesis of Inorganic Nanophase Materials in Supramolecular Protein Cages. *Nature* **1991**, *349*, 684−687.
(45) Lucon, J.; Qazi, S.; Uchida, M.; Bedwell, G. J.; LaFrance, B.; Prevelige, P. E., Jr.; Douglas, T. Use of the Interior Cavity of the p22 Capsid for Site-Specific Initiation of Atom-Transfer Radical Polymerization with High-Density Cargo Loading. *Nat. Chem.* **2012**, *4*, 781−788.
(46) Hernandez-Garcia, A.; Kraft, D. J.; Janssen, A. F. J.; Bomans, P. H. H.; Sommerdijk, N. A. J. M.; Thies-Weesie, D. M. E.; Favretto, M. E.; Brock, R.; de Wolf, F. A.; Werten, M. W. T.; et al. Design and Self-Assembly of Simple Coat Proteins for Artificial Viruses. *Nat. Nanotechnol.* **2014**, *9*, 698−702.
(47) Douglas, T.; Young, M. Host-Guest Encapsulation of Materials by Assembled Virus Protein Cages. *Nature* **1998**, *393*, 152−155.
(48) Dedeo, M. T.; Duderstadt, K. E.; Berger, J. M.; Francis, M. B. Nanoscale Protein Assemblies from a Circular Permutant of the Tobacco Mosaic Virus. *Nano Lett.* **2010**, *10*, 181−186.
(49) Durham, A. C. H.; Finch, J. T.; Klug, A. States of Aggregation of Tobacco Mosaic Virus Protein. *Nature* **1971**, *229*, 37−42.
(50) Plaza, P.; Dai Hung, N.; Martin, M. M.; Meyer, Y. H.; Vogel, M.; Rettig, W. Ultrafast Internal Charge Transfer in a Donor-Modified Rhodamine. *Chem. Phys.* **1992**, *168*, 365−373.
(51) Savarese, M.; Aliberti, A.; De Santo, I.; Battista, E.; Causa, F.; Netti, P. A.; Rega, N. Fluorescence Lifetimes and Quantum Yields of Rhodamine Derivatives: New Insights from Theory and Experiment. *J. Phys. Chem. A* **2012**, *116*, 7491−7497.
(52) Sundström, V.; Gillbro, T. Viscosity Dependent Radiationless Relaxation Rate of Cyanine Dyes. A Picosecond Laser Spectroscopy Study. *Chem. Phys.* **1981**, *61*, 257−269.
(53) Yu, A.; Tolbert, C. A.; Farrow, D. A.; Jonas, D. M. Solvatochromism and Solvation Dynamics of Structurally Related Cyanine Dyes. *J. Phys. Chem. A* **2002**, *106*, 9407−9419.
(54) Lakowicz, J. *Principles of Fluorescence Spectroscopy*; Springer: New York, 2006.
(55) Harrach, M. F.; Drossel, B. Structure and Dynamics of TIP3p, TIP4p, and TIP5p Water Near Smooth and Atomistic Walls of Different Hydroaffinity. *J. Chem. Phys.* **2014**, *140*, 174501.
(56) Laage, D.; Stirnemann, G.; Sterpone, F.; Rey, R.; Hynes, J. T. Reorientation and Allied Dynamics in Water and Aqueous Solutions. *Annu. Rev. Phys. Chem.* **2011**, *62*, 395−416.
(57) Sterpone, F.; Stirnemann, G.; Laage, D. Magnitude and Molecular Origin of Water Slowdown Next to a Protein. *J. Am. Chem. Soc.* **2012**, *134*, 4116−4119.
(58) Loparo, J. J.; Fecko, C. J.; Eaves, J. D.; Roberts, S. T.; Tokmakoff, A. Reorientational and Configurational Fluctuations in Water Observed on Molecular Length Scales. *Phys. Rev. B* **2004**, *70*, 180201.
(59) Luzar, A.; Chandler, D. Effect of Environment on Hydrogen Bond Dynamics in Liquid Water. *Phys. Rev. Lett.* **1996**, *76*, 928−931.
(60) García, A. E.; Hummer, G. Water Penetration and Escape in Proteins. *Proteins: Struct., Funct., Bioinf.* **2000**, *38*, 261−272.
(61) Egorov, A. V.; Lyubartsev, A. P.; Laaksonen, A. Molecular Dynamics Simulation Study of Glycerol-Water Liquid Mixtures. *J. Phys. Chem. B* **2011**, *115*, 14572−14581.
(62) Mark, P.; Nilsson, L. Structure and Dynamics of the TIP3p, SPC, and SPC/E Water Models at 298 K. *J. Phys. Chem. A* **2001**, *105*, 9954−9960.
(63) Joo, T.; Jia, Y.; Yu, J.-Y.; Lang, M. J.; Fleming, G. R. Third-Order Nonlinear Time Domain Probes of Solvation Dynamics. *J. Chem. Phys.* **1996**, *104*, 6089−6108.
(64) Horng, M. L.; Gardecki, J. A.; Papazyan, A.; Maroncelli, M. Subpicosecond Measurements of Polar Solvation Dynamics: Coumarin 153 Revisited. *J. Phys. Chem.* **1995**, *99*, 17311−17337.
(65) de Boeij, W. P.; Pshenichnikov, M. S.; Wiersma, D. A. Ultrafast Solvation Dynamics Explored by Femtosecond Photon Echo Spectroscopies. *Annu. Rev. Phys. Chem.* **1998**, *49*, 99−123.
(66) Asbury, J. B.; Steinel, T.; Kwak, K.; Corcelli, S. A.; Lawrence, C. P.; Skinner, J. L.; Fayer, M. D. Dynamics of Water Probed with Vibrational Echo Correlation Spectroscopy. *J. Chem. Phys.* **2004**, *121*, 12431−12446.
(67) Paarmann, A.; Hayashi, T.; Mukamel, S.; Miller, R. J. D. Probing Intermolecular Couplings in Liquid Water with Two-Dimensional Infrared Photon Echo Spectroscopy. *J. Chem. Phys.* **2008**, *128*, 191103.

DOI: 10.1021/acs.jpcb.5b03784
J. Phys. Chem. B XXXX, XXX, XXX−XXX

(68) Cowan, M. L.; Bruner, B. D.; Huse, N.; Dwyer, J. R.; Chugh, B.; Nibbering, E. T. J.; Elsaesser, T.; Miller, R. J. D. Ultrafast Memory Loss and Energy Redistribution in the Hydrogen Bond Network of Liquid H_2O. *Nature* **2005**, *434*, 199−202.
(69) Carter, E. A.; Hynes, J. T. Solvation Dynamics for an Ion Pair in a Polar Solvent: Time-Dependent Fluorescence and Photochemical Charge Transfer. *J. Chem. Phys.* **1991**, *94*, 5961−5979.
(70) Kahlow, M. A.; Jarzęba, W.; DuBruil, T. P.; Barbara, P. F. Ultrafast Emission Spectroscopy in the Ultraviolet by Time-Gated Upconversion. *Rev. Sci. Instrum.* **1988**, *59*, 1098−1109.
(71) Stenger, J.; Madsen, D.; Hamm, P.; Nibbering, E. T. J.; Elsaesser, T. A Photon Echo Peak Shift Study of Liquid Water. *J. Phys. Chem. A* **2002**, *106*, 2341−2350.
(72) Skaug, M. J.; Longo, M. L.; Faller, R. The Impact of Texas Red on Lipid Bilayer Properties. *J. Phys. Chem. B* **2011**, *115*, 8500−8505.
(73) Tinnefeld, P.; Herten, D.-P.; Sauer, M. Photophysical Dynamics of Single Molecules Studied by Spectrally-Resolved Fluorescence Lifetime Imaging Microscopy (SFLIM). *J. Phys. Chem. A* **2001**, *105*, 7989−8003.
(74) Ma, Y.-Z.; Miller, R. A.; Fleming, G. R.; Francis, M. B. Energy Transfer Dynamics in Light-Harvesting Assemblies Templated by the Tobacco Mosaic Virus Coat Protein. *J. Phys. Chem. B* **2008**, *112*, 6887−6892.

DOI: 10.1021/acs.jpcb.5b03784
J. Phys. Chem. B XXXX, XXX, XXX−XXX